Atmos. Meas. Tech. Discuss.,
doi:10.5194/amt-2020-418-AC1, 2020

Atmospheric Measurement Techniques Discussions

Interactive comment on "A Compact Rayleigh Autonomous Lidar (CORAL) for the middle atmosphere" *by* Bernd Kaifler and Natalie Kaifler

Bernd Kaifler and Natalie Kaifler

bernd.kaifler@dlr.de

Received and published: 9 December 2020

We thank the reviewer for the thorough review of our manuscript and for pointing out shortcomings in the description of the lidar system. When you are intimately familiar with an instrument, it is easy to miss something in the description which may be important to readers who are not so familiar with intricacies of that particular system. Therefore we are very grateful for the review comments and believe that by addressing those the manuscript will be greatly improved. In particular, we want to thank the reviewer for asking about the problems associated with incomplete beam overlap and focusing issues of the telescope. These are often overlooked in literature, our manuscript included. We address these problems as well as other comments in the following and will include relevant information in the revision of the manuscript.

1 The third sentence indicates that the first studies with CORAL show the impact of a strong gravity wave event on stratospheric circulation. I initially took this to mean that this paper included this analysis, but after re-reading the Discussion section I see that this is done in earlier papers. I suggest that the 3rd sentence of the abstract be modified to make this clearer (e.g 'First studies using CORAL data have shown for example...).

We agree, the sentence is indeed misleading. We will modify it in the revision to make it clear that it refers to an earlier study.

2 Please quantify the typical shot-to-shot beam pointing stability of the laser beam after divergence and comment on how this compares with the field of view of the telescope and the divergence of the transmitted beam.

We haven't measured the shot-to-shot beam pointing stability of this particular laser. The data sheet provided by the manufacturer lists $< \pm 50$ µrad as pointing stability. Expanding the beam reduces the pointing jitter to $< \pm 25$ µrad or 13.9 % of the receiving telescope FOV (361 µrad full angle; note that we falsely stated 370 µrad in the manuscript). Measurements performed with other lasers of the same manufacturer and type suggest a significantly smaller pointing jitter in the order of 25 µrad. Assuming a Gaussian distribution, the pointing jitter leads to an effective increase in the divergence of the laser beam when averaging over multiple laser shots. Assuming the upper limit of 50 µrad full angle, the effective beam divergence including the pointing jitter is 220 µrad, or 195 µrad in case of the more realistic estimate of 25 µrad pointing jitter.

3 What is the blocking level of your Raman filter at 532 nm

The specification for the out-of-band blocking of the Raman filter is optical depth (OD) >6. The dichroic mirror which separates the elastic scattering and Raman scattering has a transmission of 1.2 % at 532 nm wavelength. Both optics combined result in a blocking level of OD ~ 8 at 532 nm.

4 Given that the arrangement of the receiver and transmitter are bistatic and that the field of view of the telescope is small (370 µrad), the effect of any significant change in focus will depend on how the response function of the field of view changes and the response function of the field of view. How is the field of view of the telescope practically determined (theoretically or measured)? Please comment on the stability of the telescope focus (e.g. the significance of changes due to thermal effects)and how you determine best focus. Please also comment on if and how you can determine the significance of any range-dependent effect on the retrieved temperature profiles due to focus change.

The field of view of the telescope is given by the diameter of the fiber core a=550 µm and the focal length of the mirror $f = 2.4\,d$ ($d = 0.635$ m) (see Fig. 1):

$$\text{FOV} = \frac{5.5 \times 10^{-4}\ \text{m}}{2.4 \times 0.635\ \text{m}} = 361\ \mu\text{rad} \tag{1}$$

Note that we falsely stated 370 µrad in the manuscript.

4.1 Effect of thermal expansion

Thermal expansion and contraction of the telescope, most importantly in the z-axis or focus direction, is minimized by using carbon fiber tubes as structural member and spacer between the mirror cell and the telescope spider. The coefficient of thermal expansion of carbon fibers is -0.1×10^{-6} K^{-1} along the fiber and 21×10^{-6} m K^{-1} across. The tubes we used have 90 % of the fibers aligned along the tube and 10 % across for increased torsion stability. Thus, we assume an average coefficient of 2.09×10^{-6} m K^{-1}. Given the focal length of 1.524 m, a change in temperature of 50 K causes a focus shift of 160 µm.

We can estimate the impact of the temperature induced focus shift on the coupling efficiency as follows. First we assume that the facet of the fiber with core diameter a is fully and equally illuminated by the telescope mirror. The half angle of the illuminating light cone is then given by

$$\tan\beta = \frac{d}{2\,f}. \tag{2}$$

Next we calculate the fraction the diameter of the illuminated disk increases when the disk, previously at the position of the fiber end, is moved downward by $b = \alpha f$ where $\alpha = 2.09 \times 10^{-6}$ K^{-1} is the coefficient of thermal expansion:

$$\frac{a'}{a} = \frac{(2\,x + b)\tan\beta}{2\,x\tan\beta} = 1 + \frac{b}{2x}. \tag{3}$$

Looking at Fig. 1, the angle β can also be expressed as

$$\tan\beta = \frac{x}{2\,a}. \tag{4}$$

Eliminating $\tan\beta$ in this equation using relation (2) and substituting the result into relation (3) yields

$$\frac{a'}{a} = 1 + \frac{b\,d}{2af} \tag{5}$$

Substituting the thermal expansion $b = \alpha f$ into this equation results in

$$\frac{a'}{a} = 1 + \frac{\alpha d}{2a} = 1 + 1.21 \times 10^{-3}\ \mathrm{K}^{-1}. \tag{6}$$

Hence, we expect a 6.0 % increase in the diameter of the illuminated disk for a 50 K change in temperature. However, the fraction of the light coupled into the fiber core decreases with the diameter squared i.e. a 6.0 % increase in diameter results in a net loss of only 0.36 %. In reality, as will be shown in the next section, the signal loss is much smaller because a) the laser beam underfills the FOV of the telescope and b) more energy is concentrated in the center because of the Gaussian beam profile. We conclude that thermal expansion of the telescope has a negligible influence on the performance of the lidar.

When setting up the lidar, we scan the vicinity of the expected focus position by slowly moving up and down the fiber end using the focus motor. Because the motor is equipped with encoders, we can record the strength of the detected lidar signal in the altitude range 40-50 km as function of position. Repeated scans are performed and measurements averaged in order to reduce the effect of potential changes in atmospheric transmission during the scans. We find the optimum focus position by fitting the position of the signal maximum.

4.2 Range dependent effects

In order to evaluate range dependent effects, we look at the function $P(z)$ which describes the fraction of the collected scattered light with $1/e^2$ beam radius w passing through an aperture with radius r as function of altitude z:

$$P(z) = 1 - \exp\left(-\frac{2r^2}{w(z)^2}\right) \tag{7}$$

As aperture we define the core of the optical fiber and set $r = 0.5\,a$. The radius of the beam of scattered laser light at the location of the aperture is then given by

$$w = \frac{\epsilon}{\mathrm{FOV}} \frac{a'}{2} \tag{8}$$

where ϵ is the full-angle divergence of the imaged laser beam taken at $1/e^2$ points and FOV is the full-angle of the telescope FOV. Because the beam divergence of 170 µrad was measured at $1/e$ points we have to scale the value by 1.41. In addition, we add the effective broadening due to the pointing jitter of the laser (25 µrad) and broadening due to the point spread function of the telescope (30 µrad since the spot size of 60 µrad refers to the 2σ-value) and arrive at the beam radius of $0.408\,a'$ at the facet of the fiber.

Even if the laser beam is completely within the FOV of the telescope (full geometric overlap is achieved at 4.82 km altitude), signal may be lost due to defocusing of the telescope at low altitudes. To estimate this range dependent signal loss, we first calculate the focus shift associated with moving an object (scattered laser light) from infinity to the near vicinity of the telescope and then evaluate how this focus shift affects the coupling efficiency of telescope and fiber in a similar way as was done when analyzing the effect of thermal expansion.

Looking at Fig. 1, the angular change of the object rays is given by

$$\gamma = \frac{d}{2z}. \tag{9}$$

with z being the altitude. Here we have used the small-angle approximation $\tan\Theta \approx \Theta$. Moving the object closer i.e. increasing γ results in an increase of the focal length of the telescope by δ. The new angle

$$\beta' = \beta - \gamma \tag{10}$$

is defined by relating the new focal length to the diameter of the telescope mirror as given by

$$\tan\beta' = \frac{d}{2\,(f+\delta)}. \tag{11}$$

Solving this equation for δ and substituting relations (2), (9) and (10) yields

$$\delta = \frac{d}{2\tan\left(\tan^{-1}\left(\frac{d}{2f}\right) - \frac{d}{2z}\right)}. \tag{12}$$

Now we solve Eqn. (5) for a', replace b with the focus shift δ, and together with Eqn. (8) substitute the result into Eqn. (7):

$$P\,(z) = 1 - \exp\left(-2\frac{\mathrm{FOV}^2}{\epsilon^2}\frac{1}{\left(1+\frac{\delta\,d}{2af}\right)^2}\right) \tag{13}$$

Note that the exponential depends on the inverse of the filling factor $\epsilon\,\mathrm{FOV}^{-1}$ that describes the ratio of effective laser beam divergence and the telescope FOV, and the scaling term that takes into account the broadening of the imaged laser spot caused by the focus shift. Fig. 2 shows the altitude dependence of P and also includes two additional gray lines, the upper line marking the altitude (45 km) for which the focus position position was experimentally determined as described above, and the lower line marking our threshold of 15 km altitude. The difference in the encircled energy between the two gray lines is 1.35 %. Assuming a mean stratospheric temperature of 220km, this difference translates into a temperature error at 15 km altitude of 2.7 K. Below, the temperature error rapidly increases, as indicated by the curve in Fig. 2. For altitudes above 30 km predicted errors are below 0.3 %. The actual errors are likely smaller as suggested by a detailed comparison study which is currently in preparation

for publication and analyzes CORAL temperature profiles and ECMWF profiles in the lower stratosphere.

So far we do not attempt to correct this range dependent effect in our implementation of the temperature retrieval because, in addition to the above theoretical considerations, a more thorough experimental study of the overlap function is needed.

5 Please indicate what the expected altitude for full overlap between the fields of view of the transmitter and receiver (presumably below 14 km).

The altitude at which full overlap is achieved is defined as the point where the marginal rays of the laser beam and the telescope intersect. Given the horizontal separation of 0.4 m of the laser beam and telescope axis, the effective beam divergence of 195 µrad and the telescope FOV of 361 µrad, the intersection occurs at the altitude of 4.82 km. Full overlap is obtained for altitudes above.

6 What is the quality of the surface of the telescope in terms of RMS surface deviation (in wavelengths) from an ideal paraboloid?

We do not have any measurements of the surface quality of the telescope mirror.

7 Given that the arrangement of the receiver and transmitter are bistatic, I expect that clouds cause the conscan method to optimise the overlap for lower altitudes. Is that correct and might this cause any issues with data collection? Do you use any data in cases of cloud (even thin cloud)?

Actually, the conscan method appears to be fairly robust with regard to clouds. One major benefit over the more widely used imaging method described in Innis et al. (2007) is that the lidar return signal is analyzed well above potential cloud layers. In our implementation we evaluate the signal between 45 km and 55 km altitude. Though clouds passing through the lidar beam modulate the strength of the lidar return signal and thus impact the demodulation of the conscan error signal, this does not change the altitude for which the beam overlap is optimized. For that reason, we trust our lidar measurements and use the data in case of thin clouds. Thick clouds cause the lidar return signal to drop below a threshold and raw data profiles, we use 10 s intervals for quality checks, are automatically discarded in the temperature retrieval.

We also use quality checks in our conscan implementation. For example, we evaluate the χ^2-value retrieved from the fit (shown in Fig. 3). A large χ^2-value, we use 300 as a threshold, indicates that the conscan signal could not be properly demodulated and retrieved estimates of phase and amplitude are not reliable. In this case the conscan cycle is aborted and the beam pointing not updated. In cloudy conditions as many as 9 out of 10 conscans may fail in that way, but the succeeding conscans are still sufficient for beam tracking, as thermal drifts happen on relatively large time scales. If more than 10 successive conscans fail, subsequent intervals are marked in the raw data files as potentially having incomplete beam overlap. Moreover, beam pointing increments and conscan parameters are stored in raw data files for offline analysis. As evident from Fig. 3 only few conscan measurements exceed the the threshold of $\chi^2 > 300$ even though the lidar return signal was strongly impacted by clouds in the period 4-5 UTC. Note that we did not normalize the conscan signal prior to fitting the data. Hence, the

average χ^2-value is about 20 instead of unity even for strong conscan signals.

8 While you have a cloud-monitoring camera (discussed later) it would seem that introduction of a pellicle beamsplitter in the telescope before the fiber would allow you to monitor the quality and stability of the received beam (e.g. as done in Innis et al., 2007 -https://doi.org/10.1117/1.2801411). Could you please comment on the usefulness or otherwise of such an arrangement for data quality control.

We choose not to use a beam tracking camera as it was done in Innis et al. (2007) for two main reasons. First, pellicle beam splitters are extremely fragile and are likely not to survive for long periods in a humid environment. CORAL is located close to the coast and we operate it in marginal weather conditions such as thin fog. A plate beam splitter may solve this problem, but complicates the optical setup. Second, the addition of a beam splitter increases signal losses i.e. less light is available to the receiver. With CORAL we wanted to demonstrate that even small lidars (physical size and laser power) can produce good measurements in the mesosphere if they are optimized for low signal losses.

For some time we used a beam tracking camera looking through a separate Galilei telescope (100 mm aperture) bolted to the main telescope. We found that the error signal determined from the camera was less reliable in (partially) cloudy conditions as compared to the conscan method. We never used the camera signal to assess the data quality because we are confident in the performance of the conscan method.

9 What is the range and time separation for the SABER profile relative to the lidar measurement? Why not show a measurement centred on the time of the ECMWF profile, or is the SABER profile more coincident? What is the source of the ECMWF profile (forecast or analysis) and what is the horizontal grid resolution of the ECMWF data and separation from the measurement site?

The closest SABER profile was acquired at 525 km mean distance to the west of CORAL at 05:38 UTC. We initially chose to start the lidar integration period at the beginning of the hour, but agree that centering it at the time of the SABER profile is more appropriate. Fig. 4 shows the temperature profiles for the updated time period.

We use operational ECMWF forecast data with a grid resolution of 0.125°. The grid point closest to the location of CORAL (53.785° S, 67.752° W) is 53.75° S, 67.75° W with a distance of 3.9 km.

10 Given that you can be seeding at altitudes of 100 km or above (e.g. Fig. 12b and line 355), do you take into account the change in the mean molecular mass of the air in the MLT region, and if so, how?

No, we don't take any change in mean molecular mass into account. This is a shortcoming of our retrieval and will be addressed in the future.

11 Is the seeding altitude at the top of the retrievals in panels (b) and (c) or has allowance been made for convergence of the retrieval?

The profiles shown in Fig. 12b,c of the manuscript start 2 km below the seeding altitude. Normally you would integrate at least one density scale height to allow for the retrieved

temperature profile to converge. However, as our group mainly focuses on gravity wave studies and thus predominantly looks at perturbations with mean background temperature profiles subtracted, reaching higher altitudes is of higher importance than absolute convergence. Please note that the 2 km refers to the retrieved profile of the current level within the retrieval pyramid. For example, the 20 min profiles shown in Fig. 12c. start at ~ 90 km which is more than one density scale height below the altitude where the nightly mean profile was seeded with the SABER profile. Hence, we can assume that the seeding temperatures we used for seeding the 20 min temperature profiles 2 km above are already close to the true atmospheric temperature, allowing for rapid convergence.

12 You are describing your retrieval method in fairly general terms and I would recommend that you are more specific, referencing earlier works necessary or expanding Section 4 to more fully explain the particular criteria and assumptions that you are using. What are the coincidence criteria that you apply in the use of satellite data for seeding? Do you account for bias in the seed temperature? The averaging kernels of the MLS measurements are coarse compared to SABER in the MLT. When would you use MLS measurements to seed the profiles? How do you determine what effective height to assign to the seeding temperature obtained from MLS given that the vertical resolution of the lidar data is much less than the averaging kernel of the MLS retrieval (8-10 km)? Is the 100-108 km altitude range within the recommended upper limit for scientifically useful MLS data at your site. Is there a suitable MLS profile you can show in Fig. 8?

We assumed that the hydrostatic temperature retrieval is sufficiently described in literature and discussed only the non-standard parts specific to our implementation. However, we agree that this section should be expanded to benefit a larger audience.

As coincidence criteria we chose a maximum horizontal distance of 1000 km between the mean location of the satellite measurement and our lidar. Normally, we used SABER temperature profiles for seeding, but for rare cases when SABER data are not available, e.g. when there were problems with the instrument, we fall back to using MLS profiles. MLS seed profiles account for ~ 4 % of all seed profiles. Given the relatively large averaging kernel and temperature biases of MLS profiles in the lower thermosphere, a better approach may be the use of seed profiles derived from a SABER climatology instead of MLS data when SABER profiles are not available. In any event, we agree that substituting MLS profiles for missing SABER profiles without careful analysis may have been naive and we are grateful for the hints provided by the reviewer.

Currently we do not account for any biases satellite temperature profiles may have.

13 Can you please indicate what the SNR threshold for the far-channel corresponds to as a relative uncertainty in pseudo-density (e.g. section 1.2 in Wing et al., 2020 -https://doi.org/10.3390/atmos11010075 and Alexander et al., 2011 -https://doi.org/10.1029/2010JD015164 who use 20 % and 10 % for their seeding threshold, respectively)?

Our criterion of SNR > 4 in relation to 100 m bin width translates to a relative uncertainty in pseudo-density of 8.3 % for the default vertical resolution of 900 m and 6.5 % for 1500 m resolution.

14 By reference to earlier analysis of CORAL data, please indicate if any significant tidal signatures are present in the MLT data in Fig 12c and what characteristics of the temperature variations allow you to conclude a 5-7 hour period internal gravity wave is present (e.g. downward phase progressions or narrow duty cycle, perhaps highlighting with dashed lines).

We tried to investigate tides using the CORAL data set but had very limited success. The two main problems are that in winter temperature variability is dominated by mountain waves, and in summer, when gravity wave amplitudes are low, measurements are not long enough to capture tides. Measurements in spring indicate amplitudes of the semi-diurnal tide of <5 K up to 80 km altitude. Our amplitude estimates are consistent with amplitudes reported by Lübken et al. (2011), though we note these measurements were obtained in summer and at a higher latitude (69°S). Eckermann et al. (01 Aug. 2018) show measurements of tides acquired with the TELMA predecessor of CORAL above New Zealand with peak amplitudes of ~ 6 K at 85-90 K (their Fig. 12). Tides with similar amplitudes may be present in Fig. 5, but are certainly overshadowed by internal gravity waves which can have much larger amplitudes of 10-25 K in the upper mesosphere.

The dominating features in the mesosphere in Fig. 5 are two warm anomalies that propagate downward in time and are marked by dashed lines. Based on the observed period of ~ 5 h and 22 km vertical wavelength we conclude that these features are manifestations of internal upward propagating gravity waves.

References

Eckermann, S. D., Ma, J., Hoppel, K. W., Kuhl, D. D., Allen, D. R., Doyle, J. A., Viner, K. C., Ruston, B. C., Baker, N. L., Swadley, S. D., Whitcomb, T. R., Reynolds, C. A., Xu, L., Kaifler, N., Kaifler, B., Reid, I. M., Murphy, D. J., and Love, P. T.: High-Altitude

(0?100 km) Global Atmospheric Reanalysis System: Description and Application to the 2014 Austral Winter of the Deep Propagating Gravity Wave Experiment (DEEPWAVE), Monthly Weather Review, 146, 2639 – 2666, https://doi.org/10.1175/MWR-D-17-0386.1, https://journals.ametsoc.org/view/journals/mwre/146/8/mwr-d-17-0386.1.xml, 01 Aug. 2018.

Innis, J. L., Cunningham, A. P., Graham, A. D., and Klekociuk, A. R.: Automatically guiding a telescope to a laser beam on a biaxial antarctic light detection and ranging system, Optical Engineering, 46, 1 – 8, https://doi.org/10.1117/1.2801411, https://doi.org/10.1117/1.2801411, 2007.

Lübken, F.-J., Höffner, J., Viehl, T. P., Kaifler, B., and Morris, R. J.: First measurements of thermal tides in the summer mesopause region at Antarctic latitudes, Geophysical Research Letters, 38, https://doi.org/https://doi.org/10.1029/2011GL050045, https://agupubs.onlinelibrary.wiley.com/doi/abs/10.1029/2011GL050045, 2011.

Interactive comment on Atmos. Meas. Tech. Discuss., doi:10.5194/amt-2020-418, 2020.

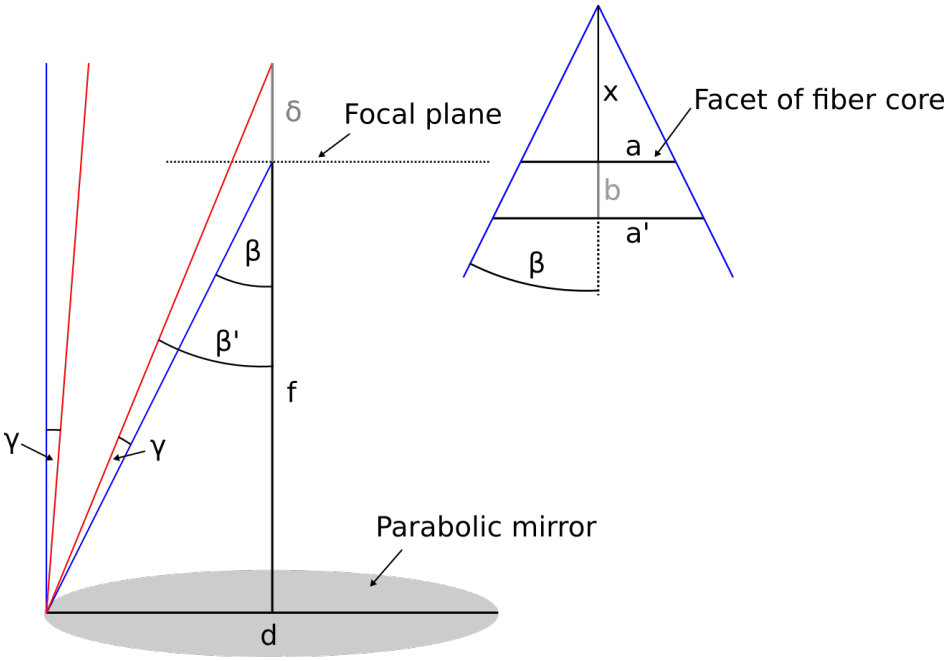

Fig. 1. Sketch showing the geometry of rays originating from infinity (blue) and near distance (red) and reflected by the telescope mirror.

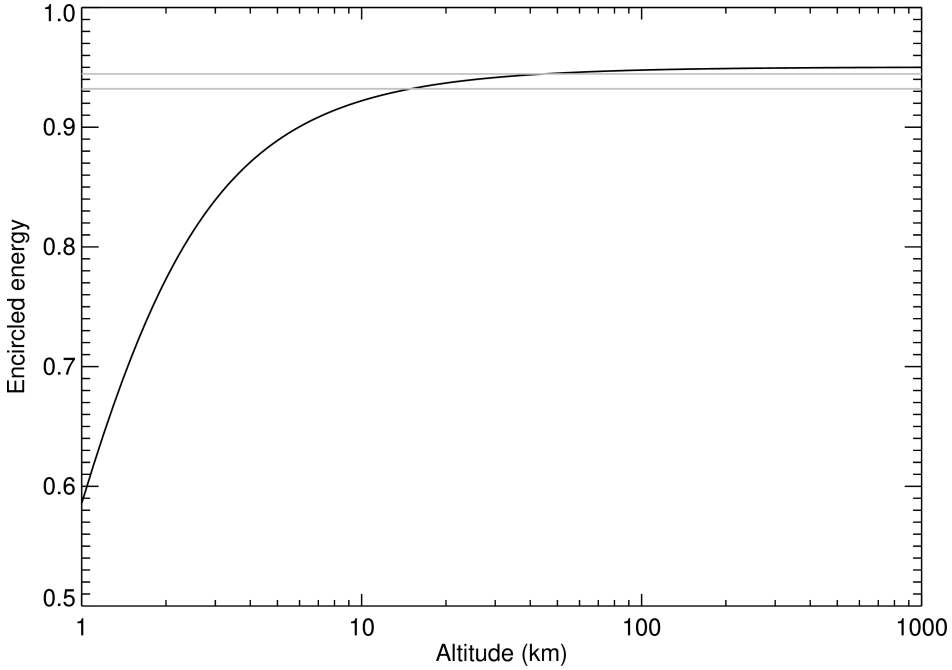

Fig. 2. Fraction of the energy passing through the aperture of the fiber core as function of altitude. The gray lines mark the focusing altitude 45 km and the threshold altitude 15 km.

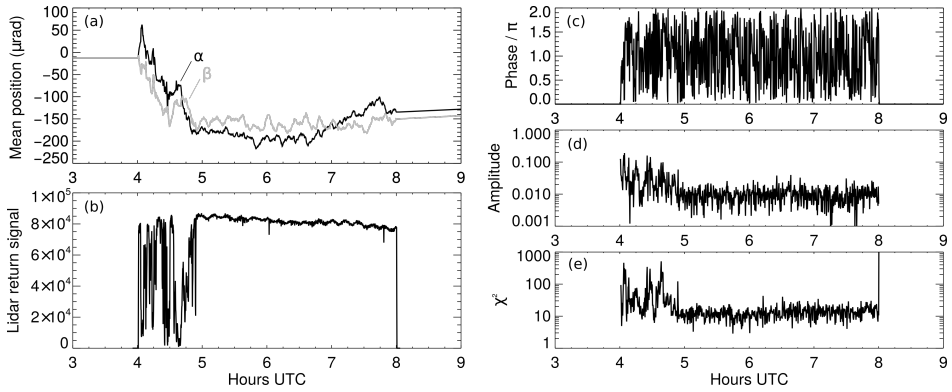

Fig. 3. Performance of the conscan system during the measurement on 3 November 2019, 4-8 UTC. (a) Scan mirror angles, (b) lidar return signal integrated between 45 km and 55 km altitude in units

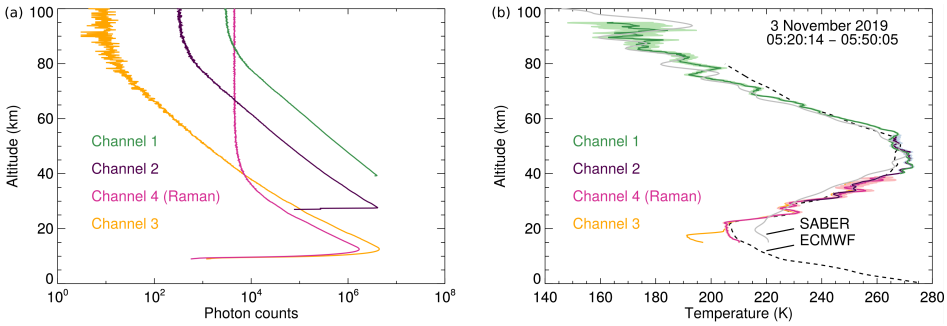

Fig. 4. (a) Photon count profiles acquired on 3 November 2019 between 05:20 and 05:50 UTC and binned to 100 m vertical resolution, and (b) retrieved temperature profiles with 900 m vertical resolution.

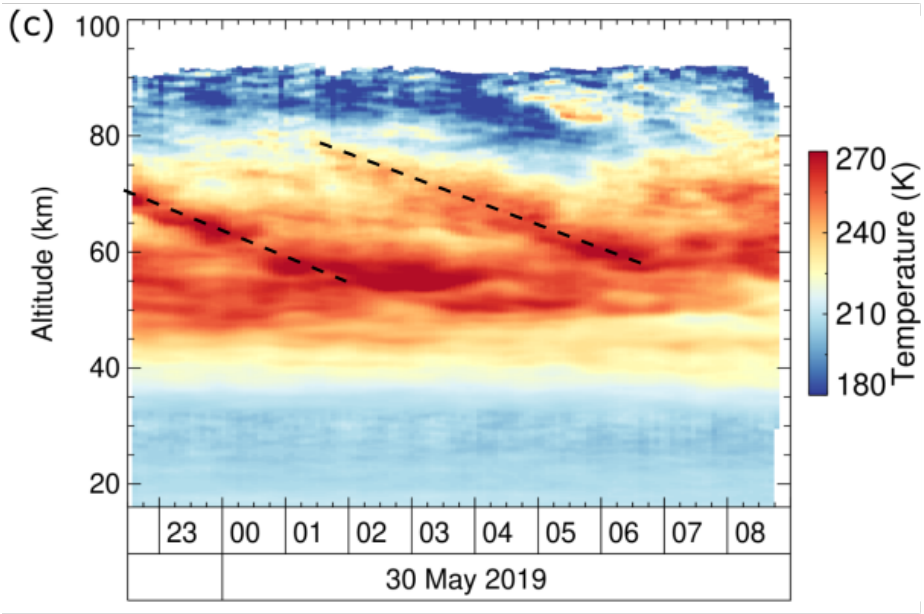

Fig. 5. Retrieved temperature profiles (original Fig. 12c in the manuscript) with gravity wave phase lines indicated by dashed lines.